



Article

Transformation, Fluxes and Impacts of Dissolved Metals from Shallow Water Hydrothermal Vents on Nearby Ecosystem Offshore of Kueishantao (NE Taiwan)

Kang Mei ^{1,2}, Deli Wang ^{1,2,*}, Yan Jiang ^{1,2}, Mengqiu Shi ^{1,2}, Chen-Tung Arthur Chen ³ , Yao Zhang ^{1,2} 
and Kai Tang ^{1,2}

¹ College of Ocean and Earth Sciences, Xiamen University, Xiamen 361005, China; meikang168@xmu.edu.cn (K.M.); jiangyan508@stu.xmu.edu.cn (Y.J.); cmbshimengqiu@cmbchina.com (M.S.); yaozhang@xmu.edu.cn (Y.Z.); tangkai@xmu.edu.cn (K.T.)

² State Key Laboratory of Marine Environmental Science, Xiamen University, Xiamen 361102, China

³ Institute of Marine Geology and Chemistry, National Sun Yat-Sen University, Kaohsiung 80424, Taiwan, China; ctchen@mail.nsysu.edu.tw

* Correspondence: deliwang@xmu.edu.cn

Abstract: Hydrothermal vents are one of the important sources of major or trace elements in the ocean. The elemental fluxes, however, may be dynamic due to coastal processes and hydrothermal plumes, especially in shallow-water hydrothermal vents. We collected water samples by using the trace-metal clean technique inside and outside two shallow-water hydrothermal vents (white vent: low temperature, high pH; and yellow vent: high temperature, low pH) off Kueishantao Islet, Taiwan, China via SCUBA divers. We analyzed these samples for their hydro-chemical parameters and dissolved elements (Fe, Mn, Mg, V, Cu, and Mo) thereafter. Our results show that dissolved metals' concentrations were significantly different between the two vents, with higher Mn and Fe in the White Vent than in the Yellow Vent, likely due to the decreased affinity of the dissolved metals for particles in the white vent. We estimated the plume fluxes of dissolved metals from the hydrothermal mouth by multiplying in situ hydrothermal discharge flowrates with metals' concentrations inside the vents, which were: $1.09\sim 7.02 \times 10^4$ kg Mg, $0.10\sim 1.23$ kg Fe, $0.08\sim 28$ kg Mn, $33.4\sim 306$ g V, $2.89\sim 77.7$ g Cu, and $54.3\sim 664$ g Mo, annually. The results further indicate that such plumes probably have impacted nearby seawater due to coastal currents and particle desorption during transport. Furthermore, the concentrations of biogenic elements could be further modified in seawater, and potentially impact nearby ecosystems on a larger scale. Our study provides information with which to further understand metal redeployment in submarine shallow nearby ecosystems.

Keywords: siderophile elements; chalcophile elements; submarine hydrothermal ecosystem; coupling processes; heavy metals; carbon; nitrogen and sulphur; Kueishantao Islet



Citation: Mei, K.; Wang, D.; Jiang, Y.; Shi, M.; Chen, C.-T.A.; Zhang, Y.; Tang, K. Transformation, Fluxes and Impacts of Dissolved Metals from Shallow Water Hydrothermal Vents on Nearby Ecosystem Offshore of Kueishantao (NE Taiwan). *Sustainability* **2022**, *14*, 1754. <https://doi.org/10.3390/su14031754>

Academic Editor: Giorgio Anfuso

Received: 10 December 2021

Accepted: 21 January 2022

Published: 3 February 2022

Publisher's Note: MDPI stays neutral with regard to jurisdictional claims in published maps and institutional affiliations.



Copyright: © 2022 by the authors. Licensee MDPI, Basel, Switzerland. This article is an open access article distributed under the terms and conditions of the Creative Commons Attribution (CC BY) license (<https://creativecommons.org/licenses/by/4.0/>).

1. Introduction

Kueishantao Islet's (KSI) shallow hydrothermal ecosystems are major sources of many chemical elements and gases in nearby coastal waters [1]. These seafloor hydrothermal vents are mostly located at the boundaries of plates (including discrete plates and converging plates), which spew gases (CO₂, H₂S, NH₃, CH₄, H₂, and SO₂) and fluids [1]. Here, magmatic fluids, seawater, and seabed bedrock interact with each other violently, along with the boundary faults or fractures, and thus hydrothermal fluids are produced with many acid-reducing sulfides and ore-forming metals [2–4]. The seabed hydrothermal system is typically characterized by layered, high-temperature, and high-salt solutions and hydrothermally active polymetallic ooze [1,5]. Once emitted, the hydrothermal fluid is further subject to mixing with ambient cold seawater, with specific microbial communities occurring in the nearby waters, and increased metal sulfide discharge and accumulation

in natural chimney bodies [6]. The unique ecosystem, here, might have a link with and potentially impact nearby ecosystems.

Siderophile metals in hydrothermal vents have been considered to be the key drivers dictating protometabolism and forming local fauna in hydrothermal systems [7,8]. In particular, siderophile–metal–ligand complexes occur in the deep ocean trenches, probably due to the combination of naturally occurring oceanic metals and ligands synthesized from the emergent CO₂, H₂, NH₃, H₂S, and H₃PO₄ [9].

Highly siderophile elements (HSE) have been used previously in tracing sulfide oxidation and thus recording the redox evolution of materials in the mantle source [10,11]. Previous studies also report that, with the discharge of metallic minerals and accumulation of sulfide, distinct microbial communities were formed as a unique photo-autotrophic ecosystem near hydrothermal vents [6]. Specifically, the microorganisms are generally more abundant in the white vents than in the yellow vents, and sox-dependent and reverse sulphate reduction are the main pathways of energy capture, with sulfide reduction as an alternative [12]. The sulfur redox bacteria generally have stronger chemolithoautotrophic ability when closer to the vent mouth, while sulfide-oxidizing bacteria are the dominant groups in the yellow vent. Both autotrophic and heterotrophic bacteria are identified occurring in these hydrothermal vents [6], although vent-fluid discharges are reported to cast harmful effects on autotrophic activities [13]. After mixing and interacting with cold seawater and seafloor rock, the hydrothermal fluids from host rocks generally contain abundant ions of Fe²⁺, Mn²⁺, silica, rare earth elements (REEs), chalcophile elements (Se, Te, As, Sb, and Hg), toxic metals Cu, Pb, Cd, and other elements (B isotope), while Mg²⁺ is consumed during particle precipitation [3,4,14–16]. Here, the elevated concentrations of residual metals might pose potential threats to the surrounding aquatic ecosystem. It has been reported that, metals (Fe and Cu) were reported to have accumulated in gills (159–175 μg g⁻¹) and hepatopancreas (59–290 μg g⁻¹) via filtration of the hydrothermal crab *Xenograpsus testudinatus*, living beside the vents in KSI [17].

Specifically, hydrothermal fluids in KSI have been reported with a record low pH value of 1.52, and a high temperature of more than 100 °C, and containing several orders of magnitude higher of Fe and Mn (2–6) than in nearby seawater [1,5]. In recent years, limited data have been reported on the total metal contents in hydrothermal fluids, mouthful plumes, nearby seawater environments, and benthic vent animals, including submarine snail *Anachis* sp. shells and the hydrothermal vent crab *Xenograpsus testudinatus* [1,4,17,18]. So far, even less data was reported regarding the dissolved metal concentrations, e.g., previous reports mentioned that hydrothermally venting elements have influenced the composition of waters and organisms nearby [6,12,16,19–22], e.g., submarine crab (Fe and Cu), marine copepods (Hg), and the abundance and composition of local zooplankton taxon [23], and even increased local plankton mortality. More recently, high contents of Fe and Mn were reported in the plumes [24]. In general, until so far, there are still limited dataset of metals reported in the hydrothermal vents, and our understanding of the transformations, impacts, and cycles of fluid-derived metals is still constrained.

This study aims to investigate the environmental parameters and dissolved siderophile metals in the hydrothermal fluids, mouthful plumes, and ambient seawater of both yellow and white vents offshore of KSI. We estimate the annual metal fluxes and evaluated the possible influences and interactions of hydrothermal vent fluids with nearby seawater. Our research explores the processes and cycling of hydrothermally derived metals and other elements from vents, and their potential impacts on the nearby ecosystem.

2. Materials and Methods

2.1. Geological Setting of the Study Area

The Kueishantao Islet (Figure 1) is located to the northeast of Taiwan, China (24.83 N, 121.96 E), about 10 km from the island coast with an area of 3 km², and belongs to the Ryukyu island arc group of the rift depression [25]. The volcanic island at the southwest Okinawa trough is at the age of about 7 ± 0.7 ka (thermoluminescence age), with the

igneous rock still active on geological activity [26]. Under the influences of the Eurasian continental plate, geological features here are complex with frequent magma activities nearby. Consequently, a specific ecosystem is formed with numerous submarine vents ~ 1 km to the southeast of the islet. In total, more than 30 vents have been reported in the area, with water depths of 10–30 m, and an active area of about 0.5 km^2 [1]. There exist three parts of its hydrothermal venting system: hillocks, formed by sulfur accumulation, natural sulfur chimney bodies, and bedrock cracks; the sulfur chimneys, which are accumulative with a large amount of natural sulfur ($>99.96\%$); and the hydrothermal sediments, which are composed of yellowish fine sulfur sand [27]. In addition, more slender sulfur columns are formed by the condensation of sulfur downward at the base of hydrothermal vents. The temperature inside the vents is generally high (as high as $116 \text{ }^\circ\text{C}$), and the water inside is commonly oxygen-enriched and acidic [27].

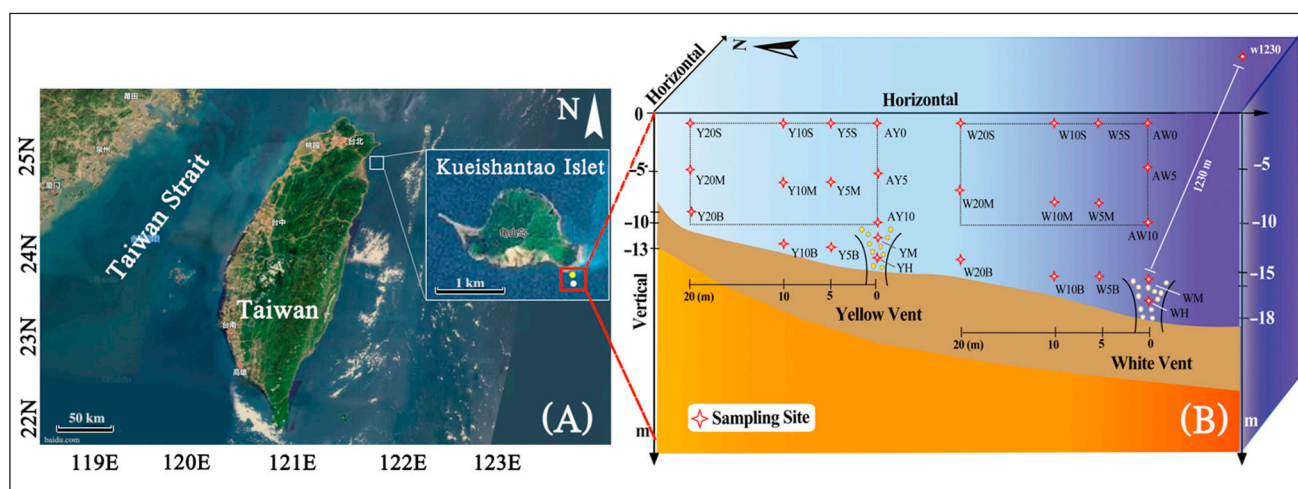


Figure 1. The satellite image and sampling sites of submarine hydrothermal areas at Kueishantao Islet (KSI) located offshore northeast Taiwan. (A) Geological location of KSI and two hydrothermal vents. The two dots refer to the locations of the yellow vent (YV, the left) and the white vent (WV, the right), respectively. (B) The four-pointed stars with labels refer to the sampling sites for seawater. Some representative labels are abbreviated as below: YH: hydrothermal fluid of the YV; YM: mouthful plume fluids of the YV; AY10: seawater sample taken 10 m above the YV; Y5S: surface seawater, taken at 5 m away from the YV; Y5M: seawater sample taken 5 m away from the YV; Y5B: seawater samples taken 5 m away from the YV bottom.

Yellow and white vents are two representative hydrothermal vents located in the southeast area of Kueishantao Islet (Figure 1A). The latest measured depths of the yellow and white vents are about 13 m and 16 m, respectively. The flow rate was $12.3 \text{ m}^3 \text{ h}^{-1}$ for the white vent, $51.5 \text{ m}^3 \text{ h}^{-1}$ for the yellow vent. Consistently, the yellow spring is characterized with higher temperature and more acidic features [5]. The hydrothermal fluids from the yellow vent generally contain a large number of yellowish sulfur particles (average $\text{pH} \approx 5.25$, $T = 90 \text{ }^\circ\text{C}$), while the white vent, discharging ivory-white fluids with a higher pH of 5.35 and lower temperature ($38 \text{ }^\circ\text{C}$).

2.2. Sampling Sites

The two submarine hydrothermal vents (yellow and white vents) are located in the Kueishantao Islet (KSI) off NE Taiwan's coast (Figure 1A). Samples from hydrothermal fluids, vertical plume, and ambient seawater were in-situ collected in titanium-made automatic gas-tight hydrothermal samplers (5 L) via scuba divers with a global positioning system on 8 August, 2017. The four-pointed stars with labels refer to the accurate sampling sites (Figure 1B). A site 1230 m (W1230) away from the white vent was chosen for sampling as reference surface seawater.

2.3. Water Sample Collection

All water samples were collected in titanium-made automatic gas-tight hydrothermal samplers (5 L). The seawater samples were collected on site and then filtered with 0.22- μm polycarbonate filters (Germany Merck Millipore Ltd., Tullagreen, Carrigtwohill, Co. Cork, Ireland) in a clean environment on board. Samples were acidified with nitric acid, and then metal ions were concentrated with Chelex-100 (Whatman, Germany) resins following the previous procedure [28,29].

2.4. Measurement and Analytical Method

The acidified samples were adjusted to $\text{pH} = 5.5$ with a diluent ammonia solution (collected and purified by using ultrapure water with AR grade) and then enriched with resins (Chelex-100 resins). The resin was rinsed with 10 mL of ultrapure water, then prepared the resin to be expanded in volume translucently with 0.1 mol L^{-1} of ammonia water, rinsed with 10 mL MQ water again, and finally the resin column was activated with 8 mL of 0.1 mol L^{-1} ammonium acetate ($\text{pH} \approx 5.5$). All samples and standard reference materials (Nearshore Seawater Reference Material for Trace Metals: CASS 5, Canada National Research Council, Ottawa, Canada) were enriched with the pre-prepared resins. The samples and the reference were eluted with 1 mol L^{-1} nitric acid, and then for measurements of trace metal elements in Fe, Mn, V, Cu, and Mo, by ICP-MS (Agilent Series 7700, Santa Clara, California, USA) [28,29]. Finally, we tested the average recovery ratios of each metal with CASS 5 (Canada National Research Council, Ottawa, Canada) and the recovery ratios are as the following: Fe (85.2–92.3%), Mn (93–99%), Cu (99–101%), V (94–98.9%), and Mo (95.5–108%).

The temperature of the hydrothermal vent was measured directly with a thermocouple thermometer (XR 440 Pocket Logger with Mvt-11 thermocouple, Pace Scientific Inc., Boone, NC, USA). The hydrothermal flux is the average flow rate measured in 5 minutes with a propeller flowmeter (Model 43-110, Hydro Bios Co Ltd., Altenholz Germany) placed on top of the vent [4]. pH was measured with a pH meter (PHM-85, Radiometer, Copenhagen, Denmark) at 25°C on board. A Guildline salinometer (Autosal 8400B, Ontario, Canada) was applied to measure and convert the conductivity to salinity (Sal.). Dissolved oxygen (DO) was directly measured with the detector in a gas chromatographic method at the day time of 10:00 AM to 13:00 PM, 8–9 August 2017. Dissolved inorganic carbon (DIC) and sulfide (H_2S) were analyzed with ion chromatographic method. The composition of gases was referred to the previous described procedure [30]. The spectrophotometric method with salicylic acid was used to measure Ammonia nitrogen (NH_4^+-N). Chlorophyll a (Chl-a) concentrations were estimated by the acetone extraction method with a Turner Designs fluorometer calibrated with pure Chl-a which purchased from Sigma Chemical Co, Ltd. (Saint Louis, MO, USA) [31].

2.5. Statistical Analysis

Data processing and statistical analysis were performed using IBM SPSS Version 23.0 (SPSS Inc., Chicago, IL, USA) and the statistics package R (V 4.1.2, 2021/11/01, <https://www.rstudio.com>, Boston, MA, USA). All data were transformed in order to reach normal distribution. The correlation of Spearman analysis was employed for analyzing the relationships between variables. Graphs were plotted via using Origin 9.0 (OriginLab Software, Northampton, MA, USA) and Prism 8 (GraphPad Software, San Diego, CA, USA).

3. Results and Discussion

3.1. Hydro-Chemical Characteristics in the Kueishantao Field

The geochemical characteristics of the plume and ambient seawater are presented in Figure 2. The results were further depicted by comparing the two vents. The parameters are listed below: temperature ($T^\circ\text{C}$) dissolved oxygen (DO), salinity, sulfide (S), nutrients

($\text{NH}_4^+\text{-N}$), pH, total alkalinity (TA), dissolved inorganic carbon (DIC), and chlorophyll a (Chl-a). The distribution of these environmental parameters is shown in the Figure 3.

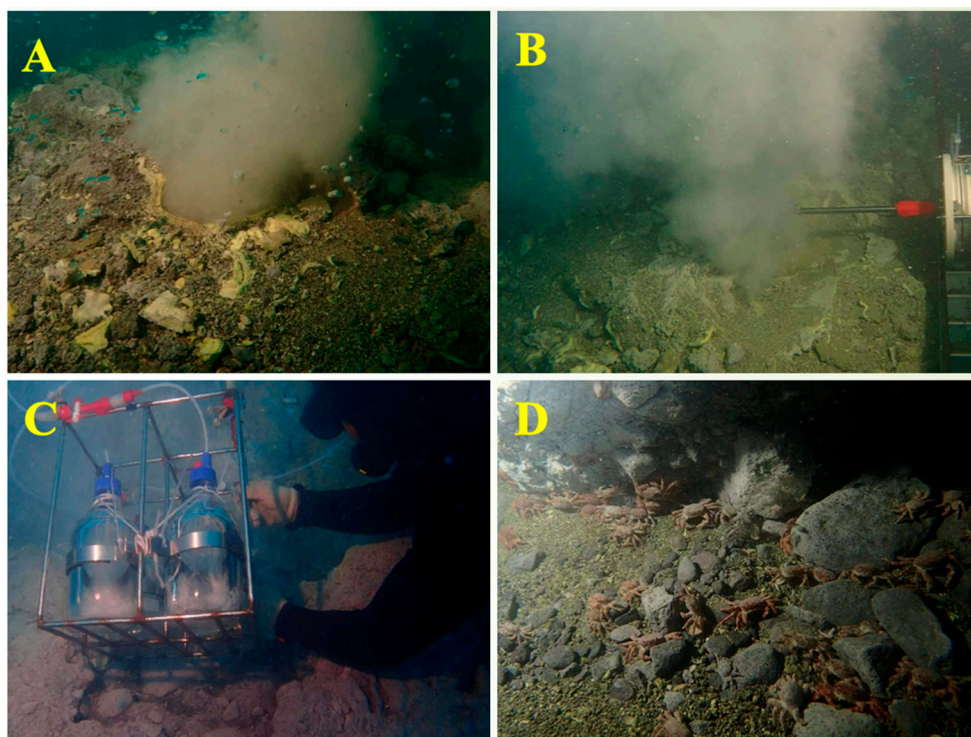


Figure 2. Some examples of fieldwork photos: (A) the yellow vent, (B) the white vent, (C) seawater sampling, and (D) vent crabs *Xenograpsus testudinatus* in Kueishantao hydrothermal field (Note: photos provided by the Seawatch Co. Ltd.).

The results show that the temperature in the yellow vent (50–90 °C) was significantly higher than that in the white vent (31–38 °C), as consistent with historic records (range: 70–116 °C) [1]. DO was characterized by low concentrations in both vents as Figure 2B, but was lower in the yellow vent than in the white vent. The low concentrations of DO and the high sulfide concentrations has been commonly observed previously in the yellow vent [1]. The chimney body of the yellow vent is composed of abundant sulfides, while the hydrothermal fluid there contain high abundance of sulfur particles. Accordingly, dissolved sulfide in the YH (0.58 mg kg⁻¹) was much lower than that in the hydrothermal mouth (11.75 mg kg⁻¹) of the yellow vent, while it varied slightly in the white vent (7.1–7.6 mg kg⁻¹).

There exist complex geochemical reactions (including precipitation) when hydrothermal fluids were mixed with cold and alkaline seawater nearby [2]. Microorganisms such as *Thiomicrospira*, *Thiomicrothrix*, *Thiothrix*, *Sulfurovum*, and *Arcobacter* likely derive energy through the oxidation of reduced sulfide and then fix dissolved inorganic carbon (DIC) by the Calvin or reverse tricarboxylic acid cycles [12].

The salinity was about 33.73 in the yellow vent, higher (33.59 and 33.72) in the white vent. The pH values both show an increasing trend from the hydrothermal fluid to plumes and then further increasing until the ambient seawaters (Figure 3F).

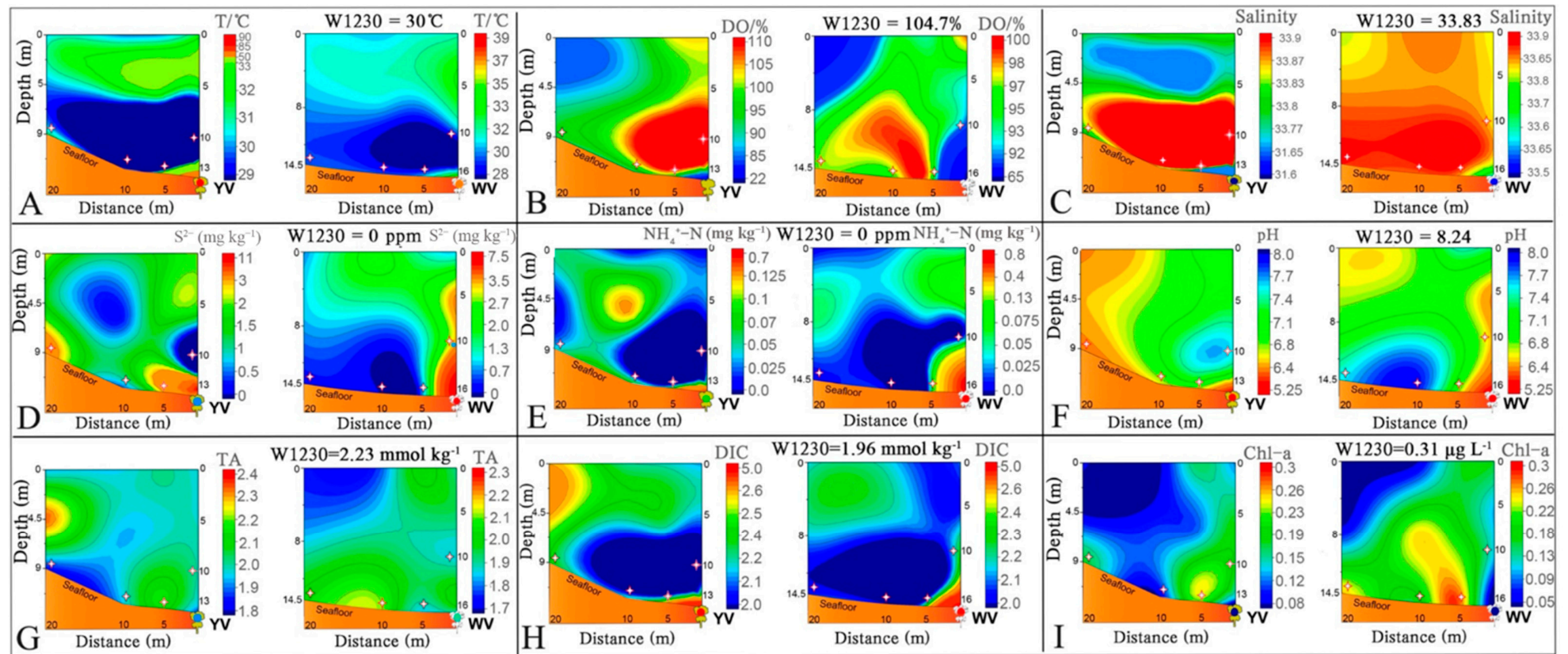


Figure 3. The distribution of environmental factors around the yellow vent (YV) and the white vent (WV) in the Kueishantao hydrothermal field. (A): Temperature (T); (B): dissolved oxygen (DO); (C): salinity; (D): sulfate concentration (S^{2-}); (E): total ammonia nitrogen of nutrient (NH_4^+-N); (F): pH; (G): total alkalinity (TA); (H): dissolved inorganic carbon (DIC); (I): chlorophyll a (Chl-a). W1230 is the value of seawater away 1230 m from the WV.

The concentrations of $\text{NH}_4^+\text{-N}$ was much higher inside the yellow vent than that in the vent mouth ($0.7 \text{ mg kg}^{-1} > 0.07 \text{ mg kg}^{-1}$), while the concentrations were much close around the white vent ($0.74\text{--}0.82 \text{ mg kg}^{-1}$). In addition, $\text{NH}_4^+\text{-N}$ was comparatively lower at the nearby site (W1230). The distribution of TA and DIC was the opposite: TA in the yellow vent ($1866\text{--}1968 \text{ } \mu\text{mol kg}^{-1}$) and in the white vent ($1925\text{--}2060 \text{ } \mu\text{mol kg}^{-1}$) were both less than those in the vent plumes. DIC in the yellow vent (YH: $5078 \text{ } \mu\text{mol kg}^{-1} > \text{YM: } 2644 \text{ } \mu\text{mol kg}^{-1}$) and in the white vent (WH: $4829 \text{ } \mu\text{mol kg}^{-1} > \text{WM: } 3738 \text{ } \mu\text{mol kg}^{-1}$) were both higher than in the vent plumes. The Chl-a content in the yellow vent ($0.13 \text{ } \mu\text{g L}^{-1}$) was higher than that in the white vent ($0.01 \text{ } \mu\text{g L}^{-1}$), which were both lower than that (W1230 = $0.31 \text{ } \mu\text{g L}^{-1}$) in the nearby site. Chl-a was not detected inside the two hydrothermal fluids.

3.2. Siderophile Metal Characterization of Hydrothermal Vents

The vent fluids inside the yellow vent and the white vent were characterized with lower siderophile metal concentrations than in hydrothermal mouthful plumes and ambient vertical seawater, while Fe and Mn show the opposite in the yellow vent (Figure 4). The dissolved Fe inside of the white vent and its vent mouth was twice as great as that in the yellow vent, respectively. Fe content in the white vent mouth was as high as $108.05 \text{ nmol L}^{-1}$, while lower in the yellow vent mouth ($24.61 \text{ nmol L}^{-1}$). In general, the concentrations of dissolved Fe were higher in the white vent than in the yellow vent, while dissolved Fe was lowest in the nearby site W1230 ($16.82 \text{ nmol L}^{-1}$). Dissolved Mn was quite abundant but subject to precipitate out rapidly in the hydrothermal fluid, and the plume outside the yellow vent showed with a low value ($31.66 \text{ nmol L}^{-1}$) (Figure 4). The concentrations of dissolved Mn inside the white vent ($4630.2 \text{ nmol L}^{-1}$) and the vent mouth ($1770.1 \text{ nmol L}^{-1}$) were significantly higher than that in the surrounding seawater ($147.56 \text{ nmol L}^{-1}$), indicative of an addition of the metal during being transported. In comparison, the yellow vent showed with much lower Mn, and the order of Mn concentrations was shown in the Figure 4: YH (inside) $>$ YM (mouth) $>$ W1230 (5.03 nmol L^{-1}) $>$ AY10 (above = 3.77 nmol L^{-1}), probably due to the fact of particle removal outwards. Previous researchers reported that investigated total Mn ($1.15\text{--}2.01 \text{ } \mu\text{mol L}^{-1}$) and total Fe ($7.12\text{--}2.01 \text{ mmol L}^{-1}$) including both dissolved and particulate forms in the two hydrothermal fluids could mostly occur in the unfiltered fraction [32].

Dissolved V ranged from $6.07\text{--}17 \text{ nmol L}^{-1}$, Cu, from $0.45\text{--}6.39 \text{ nmol L}^{-1}$, and Mo ranged from $1.25\text{--}40.04 \text{ nmol L}^{-1}$ inside the vents, showing a correlation with each other. The concentrations of dissolved V ($14.84 \text{ nmol L}^{-1}$), Cu (3.04 nmol L^{-1}), and Mo ($67.41 \text{ nmol L}^{-1}$) were observed in the nearby site W1230. The salinity ($R^2 = 0.924$), DIC ($R^2 = 0.95$), and $\text{NH}_4^+\text{-N}$ ($R^2 = 0.63$) were linearly correlated with the dissolved V ($p > 0.05$, Figure 5). The elevated metals (Figure 4) might be attributable to a series of geochemical reactions, including chloride-induced desorption from suspended particles (Figure 3C), the oxidation of metal sulfides (Figure 3D), and the partial dissolution of Fe-rich minerals [28,33]. The low salinity in the yellow vent (Figure 5) may have resulted from either phase separation or the intrusion of meteoric groundwater from KSI island [4,5]. The mixing with seawater along with particle precipitation acted as the main process dictating the metal variations in the hydrothermal fluids, plumes, and seawaters. Additionally, the conditions of high temperature and low pH may have favored the increased concentrations of dissolved metals [17], e.g., V and Mo. The relatively higher dissolved metal concentrations in the white vent mouthful plumes could be attributable to the mixing process with penetrated seawater before venting [4]. In addition, the lower concentration of S, Fe, and Mn, the higher content of DIC and $\text{NH}_4^+\text{-N}$ in the yellow and white vents, indicating that the above mentioned elements may have been precipitated (Fe, Mn, and S; Figures 3D and 4) or been consumed (C and N; Figure 3E,H) via geochemical reactions with or without biological involvement (autotrophic and heterotrophic bacteria of sulfur oxidation and carbon fixation) in the shallow-sea hydrothermal seafloor before release [6].

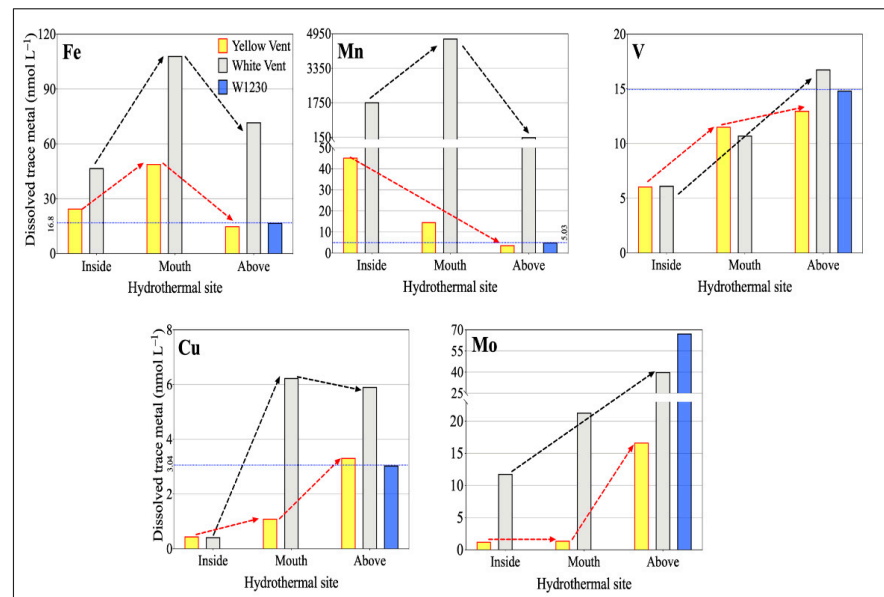


Figure 4. Dissolved metals' concentrations in hydrothermal vent fluids, plumes and seawater sites from the yellow vent and white vent in the Kueishantao area. Inside: hydrothermal fluid of two vents (YH/WH); mouth: mouthful plume fluids of two vents (YM/WM); above: ten-meter depth plume seawaters above two vents (AY10/AW10); blue bar: nearby site away 1230 m from the white vent (W1230).

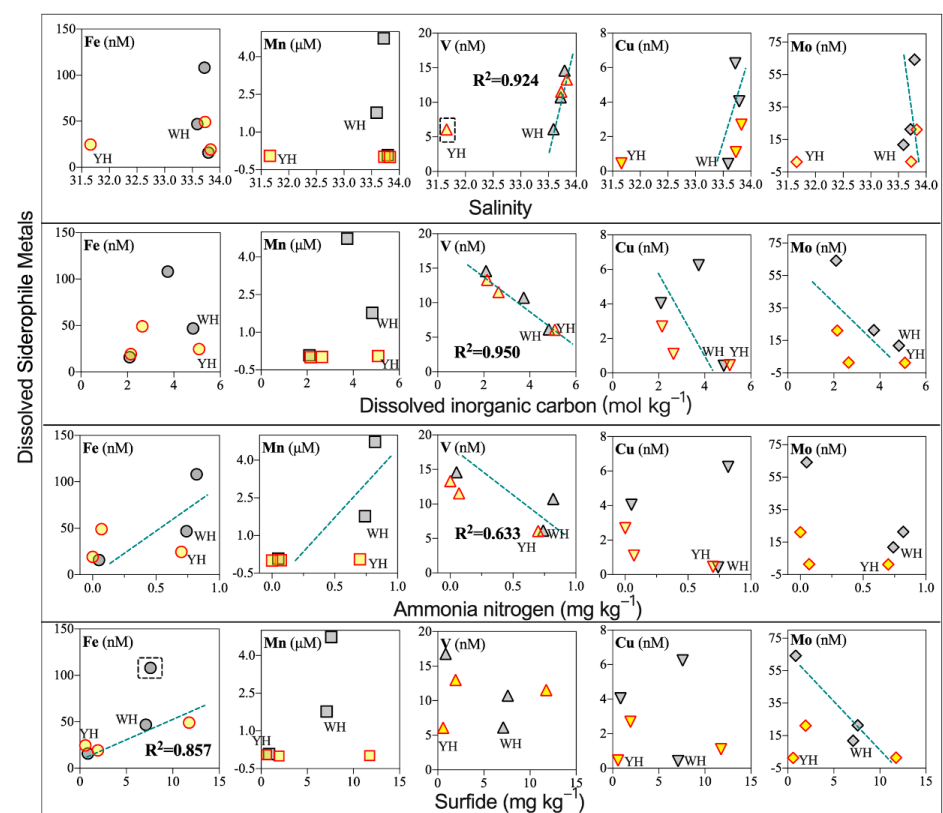


Figure 5. Characteristics of siderophile metals (Fe, Mn, V, Cu, and Mo) along with increasing salinity, dissolved inorganic carbon, ammonia nitrogen, and sulfide in the yellow and white vent hydrothermal fluids and two plume sites in the Kueishantao area. The vent fluids from the yellow vent (YV) and the white vent (WV) are both labeled. The linear fits were calculated by discarding the data of dotted box.

Fe and Mn showed similar distribution patterns, as both metals exhibited the highest concentrations in mouthful plumes (except Mn for the yellow vent), and both contents declined in the sites above the vents, the enrichment of the two metals within the vents might be attributable to submarine vent releasing [4]. The major ion Mg inside the vents ($0.99\text{--}2.33\text{ mmol L}^{-1}$) was lower than in the nearby seawater ($W1230 = 3.84\text{ mmol L}^{-1}$), as it was largely depleted via precipitation [4,34].

The influence of seawater mixing was demonstrated in the profiles of the environmental parameters in the yellow and white vent plumes (Figure 3). Additionally, the flux of the yellow vent (up to $51.5\text{ m}^3\text{ h}^{-1}$) was much higher than that of the white vent ($12.3\text{ m}^3\text{ h}^{-1}$), which served as another factor dictating the metals' distribution. Likely, the white vent's buoyant plumes were still influenced from the nearby yellow vent plumes [4]. The biogeochemical processes may contribute to the variations of metal concentrations from the hydrothermal fluids to buoyant plumes and ambient seawaters, which include the modulation from marine life, seawater dilution, coprecipitation, phase separation, scavenging or removing by Fe- and Mn-rich particles, and so on [4,6,32].

3.3. Plume Fluxes of Dissolved Metals from the Hydrothermal Vents

We further explored the potential impacts of hydrothermal plumes on ambient coastal seawaters, especially on the submarine ecosystem off the Kueishantao Islet. We measured the concentrations of dissolved metals (Fe, Mn, V, Cu, and Mo) and a major element of Mg (Table 1) in the hydrothermal fluid, ambient plumes, and vertical profile of seawater in the yellow and white vents. Previous surveys on the metals in the hydrothermal vent fluids, plumes, snail shells *Anachis* sp., and crab *Xenograpsus testudinatus* are listed in the Table 1. The elements in the two vents were relatively abundant, as released from the hydrothermal fluids outwards. Consistently, our research also showed that several metals (Fe, Mn, and Cu) exhibited sufficient exports to the surrounding seawater environments [1,4]. The total Fe and Mn in the hydrothermal fluids from the white vent ($35.7\text{ }\mu\text{mol L}^{-1}$) were both much higher than that from the yellow vent ($7.13\text{--}7.86\text{ }\mu\text{mol L}^{-1}$, Table 1). Therefore, the metal-enrichment obviously altered the elemental composition of nearby marine life, as high bioaccumulation of Fe ($37.04\text{--}175\text{ }\mu\text{g g}^{-1}$) and Cu ($53.4\text{--}290\text{ }\mu\text{g g}^{-1}$) were detected in the crab and snail as Table 1 [17,18].

To better explore the impacts of siderophile metals, the flow rates of the vents were used to assess the flux influence on the ambient waters and its potential threats to the submarine ecosystem. It was recorded with the flux of the yellow vent fluids of up to $150\text{ m}^3\text{ h}^{-1}$, larger than that of the white vent fluids ($<7\text{ m}^3\text{ h}^{-1}$) in May 2011 [4]. Our previous work showed the flux of the yellow vent had a lower flow rate ($97.5\text{ m}^3\text{ h}^{-1}$), while the higher flow rate ($12.3\text{ m}^3\text{ h}^{-1}$) of the white vent was observed in May 2015 (unpublished). In this study, the flow rate was measured in August 2017 with the rate of up to $51.5\text{ m}^3\text{ h}^{-1}$ in the yellow vent, and $12.3\text{ m}^3\text{ h}^{-1}$ in the white vent (Figure 6). Such slight changes in flow rate might be attributable to the effects of earthquakes [35]. Here, dissolved siderophile metals (Fe, Mn, V, Cu, and Mo) and major elements (Mg and Ca) are discussed as assessments the environmental processes due to hydrothermal activities summarily.

The equation for assessing the annual metal flux (AMF) of the yellow vent and the white vent releasing into the ambient waters (kg or g) is expressed as the following:

$$\text{Annual Metal Flux (AMF)} = f_m \times C_m \times 24 \times 365 \quad (1)$$

where f_m is the flow rate ($\text{m}^3\text{ h}^{-1}$) of hydrothermal vents, C_m is the concentration of dissolved trace metals (nmol L^{-1}).

Table 1. The annual flux of dissolved trace elements in yellow vent and white vent near Kueishantao Islet located offshore from northeast Taiwan, and historic data (nM = nmol L⁻¹; μM = μmol L⁻¹, mM = mmol L⁻¹).

Study Area	Sampling Site	Type	Fe	Mn	V	Cu	Mo	Ca	Mg
Kueishantao [1]	hot T (°C) plumes	seawater in total	22.3 ± 32.8 μM	1.31 ± 2.43 μM	-	218 ± 862 μM	-	9.43 ± 0.50 mM	48.7 ± 2.25 mM
	low T (°C) plumes	seawater in total	7.92 ± 6.55 μM	0.58 ± 0.51 μM	-	5.25 ± 8.52 μM	-	9.64 ± 0.36 mM	49.8 ± 1.52 mM
Kueishantao [17]	<i>Xenograpsus testudinatus</i> (crab in D.W.)	gill (μg g ⁻¹ D.W.)	159 ± 71.0	3.31 ± 1.31	-	290 ± 91.41	-	-	-
		hepatopancreas (μg g ⁻¹)	175 ± 99.2	3.95 ± 2.35	-	53.4 ± 37.6	-	-	-
		muscle (μg g ⁻¹ D.W.)	37.04 ± 21.72	0.69 ± 0.5	-	74.6 ± 27.1	-	-	-
Kueishantao [4]	surface seawater	total (unfiltered)	1.96–7.74 μM	0.78–1.19 μM	-	-	-	10.6–12.5 mM	51.1–55.5 mM
	yellow vent fluids	total (unfiltered)	7.13–7.86 μM	1.14–1.15 μM	-	-	-	10.0–10.3 mM	50.1–50.9 mM
	yellow vent plume	total (unfiltered)	9.13–13.6 μM	1.37–1.43 μM	-	-	-	10.3–10.5 mM	50.5–50.6 mM
	white vent fluids	total (unfiltered)	35.7 μM	2.01 μM	-	-	-	9.2 mM	48.4 mM
	white vent plume	total (unfiltered)	4.19–6.54 μM	0.96–1.42 μM	-	-	-	10–10.2 mM	50.2–52.4 mM
Kueishantao [18]	<i>Xenograpsus testudinatus</i>	male crab's back	32.1–55.9 μg g ⁻¹	4.77–14.6 μg g ⁻¹	-	1.53–3.21 μg g ⁻¹	-	30.1–31.7%	1.72–2.02%
		female crab's back	35.0–67.4 μg g ⁻¹	3.60–6.0 μg g ⁻¹	-	2.21–4.25 μg g ⁻¹	-	30.9–31.8%	1.52–1.94%
		male crab's claw	14.0–73.0 μg g ⁻¹	3.60–7.55 μg g ⁻¹	-	1.61–2.33 μg g ⁻¹	-	30.4–31.5%	1.50–1.96%
		female crab's claw	47.0–55.9 μg g ⁻¹	4.06–4.62 μg g ⁻¹	-	3.52–4.02 μg g ⁻¹	-	30.2–30.6%	1.84–1.94%
	snail (<i>Anachis</i> sp.)	shell (mg g ⁻¹)	53.7–108 μg g ⁻¹	4.72–8.89 μg g ⁻¹	-	4.05–4.40 μg g ⁻¹	-	39.2–40.6%	146–330 μg g ⁻¹
this study (2017)	fluid	dissolved (nM)/Flux	24.6/0.62 kg	45.4/1.13 kg	6.07/139 g	0.45/12.9 g	1.25/54.3 g	-	0.99 mM/4.28 × 10 ⁴ kg
yellow vent	plume	dissolved (nM)/Flux	49.0/1.24 kg	14.7/0.36 kg	11.5/266 g	1.10/31.7 g	1.42/61.6 g	-	1.29 mM/5.59 × 10 ⁴ kg
	seawater	dissolved (nM)/Flux	19.2/0.49 kg	3.14/0.08 kg	13.3/306 g	2.69/77.7 g	21.1/915 g	-	1.62 mM/7.02 × 10 ⁴ kg
	fluid	dissolved (nM)/Flux	46.8/0.28 kg	1770/10.5 kg	6.13/33.7 g	0.42/2.89 g	11.8/122 g	-	1.09 mM/1.13 × 10 ⁴ kg
white vent	plume	dissolved (nM)/Flux	108/0.65 kg	4730/28.0 kg	10.7/59.0 g	6.24/43.1 g	21.3/221 g	-	2.33 mM/2.41 × 10 ⁴ kg
	seawater	dissolved (nM)/Flux	15.8/0.1 kg	80.5/0.48 kg	14.6/80.2 g	4.04/27.9 g	64.2/664 g	-	1.34 mM/1.39 × 10 ⁴ kg

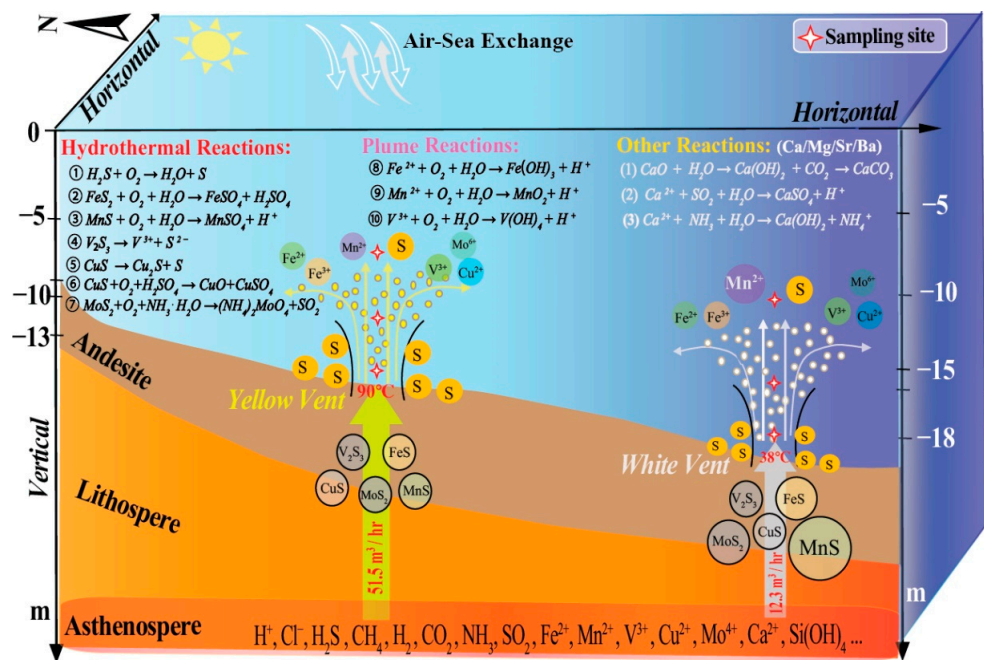


Figure 6. Schematic diagram of hydrothermal metal circulation and interaction with hydrothermal vent fluids in the submarine hydrothermal field based on the present study.

The estimated annual fluxes of dissolved elements emanating from the hydrothermal vents are in the following ranges: $1.09\text{--}7.02 \times 10^4$ kg Mg, 0.10–1.23 kg Fe, 0.08–28 kg Mn, 33.4–306 g V, 2.89–77.7 g Cu, and 54.3–664 g Mo (Table 2). It should be mentioned that there are more than 30 individual hydrothermal vents in the KSI field; our estimates might be lower than their actual influence on their ambient environments, e.g., plankton mortality covers possibly more than 1.5%, which poses great challenges for local marine organisms, [19,21]. The metals (Fe and Cu) accumulated in gills and hepatopancreas of the hydrothermal crab *Xenograpsus testudinatus*, which lives by the sides of these vents via filtration [17]. In general, hydrothermal venting at KSI Island contribute to siderophile metals inputs of ambient seawater; the influence on the nearby environment is quite limited and localized due to the large volume of seawater dilution, which is consistent with previous report [4].

Table 2. The correlations among the determined parameters in the yellow vent and the white vent. The significant correlations at 0.05 and 0.01 levels are marked in bold.

	Salinity	S	NH ₄ ⁺	pH	TA	DIC	Chl-a	Fe	Mn	V	Cu
salinity	1										
S	0.143	1									
NH ₄ ⁺	−0.771	0.314	1								
pH	0.943^b	0.086	−0.714	1							
TA	0.657	0.371	−0.086	0.600	1						
DIC	−0.943^b	−0.086	0.714	−1.00^b	−0.60	1					
Chl-a	0.812^a	0.174	−0.638	0.928^b	0.464	−0.928^b	1				
Fe	−0.429	0.771	0.771	−0.486	0.143	0.486	−0.348	1			
Mn	−0.486	0.143	0.829^a	−0.314	0.143	0.314	−0.319	0.429	1		
V	0.943^b	0.086	−0.714	1.00^b	0.600	−1.00^b	0.928^b	−0.486	−0.314	1	
Cu	0.543	0.143	−0.086	0.600	0.886^a	−0.600	0.580	0.029	0.200	0.600	1
Mo	0.600	0.029	−0.143	0.714	0.771	−0.714	0.551	−0.257	0.371	0.714	0.771

Note: ‘a’ refers to correlation at the 0.05 level being significant (two-tailed); ‘b’ refers to the correlation at the 0.01 level being significant (two-tailed).

3.4. Geochemical Implications and Possible Processes Dictating Dissolved Metals

The trace metals (V, Cu, and Mo) were positively correlated with salinity, pH, TA, and Chl-a, but negatively correlated with DIC, all with correlation coefficients of above 0.54 (significant at 0.05 level), suggesting that these parameters behaved coherently during fluid venting and seawater mixing (Table 2). Fe ($R^2 = 0.77$) and Mn ($R^2 = 0.83$) also displayed a positive correlation with $\text{NH}_4^+\text{-N}$, indicating the NH_4^+ concentration was restrained by the behavior of Fe and Mn, as well as by the seawater dilution.

To reveal the regional dynamics of trace metals and environmental factors in the yellow vent and the white vent, principal component analyses (PCA) were applied using the determined parameters as shown in the Figure 7. The classification and interpretation of siderophile metals and environmental characteristics were further assessed by PCA analyses. The first two principal components explained 40.4% (PC1) and 21.8% (PC2) of the variances, respectively, the determined parameters of the two vents can be classified into two components with a total cumulative variance of 63% (Figure 7).

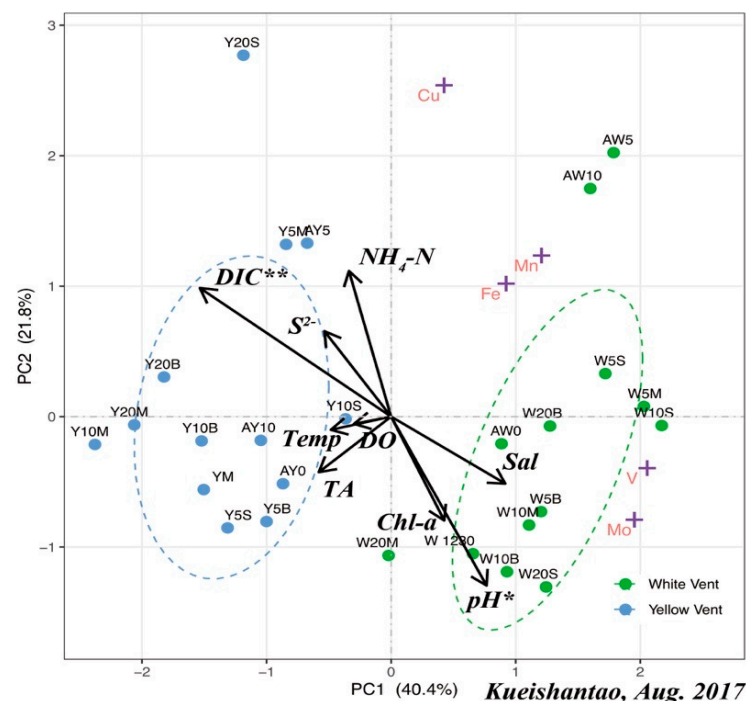


Figure 7. Principal component analyses based on the results of siderophile metals concentrations and the environmental factors of hydrothermal vent fluids from the yellow vent and the white vent.

Samples of the yellow vent were grouped along the negative axis of PC1, while the positive for the white vent. V and Mo with negative loading and Fe, Mn, and Cu with moderately positive loadings composed the second component (PC2). The samples of the yellow vent had high loadings on temperature, DIC, S, and NH_4^+ . The enrichment and content ratios of the chalcophile elements (Se, Te, As, Sb, and Hg) demonstrated their abundance in the sulfur matrix and minor fractionation after being partitioned into the metallic melt and forming a separate vapor phase to transport [16]. The DIC results are highly related to the variation of seawater pH, which might indirectly affect the metal behavior, and the primary producer utilizes CO_2 to perform photosynthesis. In addition, five selected metals show positive loadings with environmental factors in PC1. Those samples from the white vent have high loadings on pH, salinity, TA, and Chl-a. In these environmental factors, the greater the total alkalinity (TA), the more hydroxide radicals (OH^-) is. Thus, it becomes easier for adsorption and precipitation processes of dissolved metals in these hydrothermal vents. Consistently, previous research show that particulate organic carbon was enriched in the vertical plumes as explained by physicochemical

processes rather than biological sources [36]. In addition, microorganisms might also alter the abundance of trace metals in seawater surroundings.

We assume that dissolved metals might change due to phase fractionation, partially, as the schematic diagram illustrates in Figure 6. The content of Chl-a was highly associated with the content of trace metals (V, Cu, and Mo) (Table 2, $R^2 > 0.55$), and these metals shows a relationship with environmental characteristics, including salinity, pH, TA, and DIC (negative correlation). DIC ($p < 0.01$) and pH ($p < 0.05$) show significant differences in samples (Figure 7). There was no significant correlation ($p > 0.05$) between siderophile metals and the S except Fe (Table 2, $R^2 = 0.77$), suggesting that the element might originate from hydrothermal venting and be diluted by ambient seawater.

4. Conclusions

In this study, we, for the first time, collected samples inside the two vents (yellow and white) from Kueishantao Islet, Taiwan, China, and analyzed the samples for their content of dissolved metals, including Fe, Mn, Cu, V, and Mo. The two vents show a large difference in terms of hydro-chemical parameters. For example, the yellow vent was characterized by a higher temperature (90 °C) and lower pH, higher plume-discharging rate, while the white vent by lower temperature, higher pH, and lower plume discharge rate. Both vents contained a large number of sulfide particles and element sulfur.

In particular, our results show a significant difference in dissolved metals' concentrations among the two vents, and also in the surrounding sites. Higher releases of dissolved metals in the white vent than in the yellow vent might be attributed to more precipitation occurring in the yellow vent, as dissolved Fe and Mn concentrations are elevated in all sampling stations, probably due to increased desorption from particles, while the concentrations of dissolved V, Cu, and Mo were also altered during the hydrothermal processes and the following geochemical reactions. The flux of dissolved Fe and Mn contributed to the ambient environment significantly, while V, Cu, and Mo may be substantially removed within hydrothermal processes during particle adsorption and precipitation.

In addition, the hydrothermal systems were characterized by a large number of acid-reducible sulfides, ore-forming metals, and highly toxic and acidic hydrothermal fluids, which dictated a quite distinct ecosystem from the nearby coastal environment. These results reveal that submarine hydrothermal venting might have already contaminated the adjacent seawater and further affected the local environment and marine organisms.

In summary, our research here reports a dataset of dissolved metals (Fe, Mn, Cu, V, and Mo) inside the two shallow-water hydrothermal vents. The concentrations of these metals were altered in nearby seawater, as a result of combination of coastal and hydrothermal processes. Our data further hints at a preliminary insight for the siderophile metal processes of fluid–plume–seawater interactions, and an enlightening understanding of the metal redeployment in the submarine shallow nearby ecosystem.

Author Contributions: Conceptualization, D.W.; methodology, D.W.; software, K.M.; validation, D.W. and K.M.; formal analysis, D.W. and K.M.; investigation, Y.J. and M.S.; resources, D.W., C.-T.A.C., Y.Z., and K.T.; data curation, D.W. and K.M.; writing—original draft preparation, D.W. and K.M.; writing—review and editing, D.W. and K.M.; visualization, K.M.; supervision, D.W.; project administration, Y.Z.; funding acquisition, D.W., C.-T.A.C., Y.Z., and K.T. All authors have read and agreed to the published version of the manuscript.

Funding: This research is funded by the programs U1805242 and #41676070 of National Natural Science Foundation of China (NSFC).

Acknowledgments: We would like to thank State Key Laboratory of Marine Environmental Science, Xiamen University for the full support and the people who helped us during the cruise.

Conflicts of Interest: The authors declare no conflict of interest.

References

1. Chen, C.T.A.; Zeng, Z.G.; Kuo, F.W.; Yang, T.Y.F.; Wang, B.J.; Tu, Y.Y. Tide-influenced acidic hydrothermal system offshore NE Taiwan. *Chem. Geol.* **2005**, *224*, 69–81. [[CrossRef](#)]
2. Koschinsky, A.; Garbe-Schonberg, D.; Sander, S.; Schmidt, K.; Gennerich, H.H.; Strauss, H. Hydrothermal venting at pressure-temperature conditions above the critical point of seawater, 5° S on the Mid-Atlantic Ridge. *Geology* **2008**, *36*, 615–618. [[CrossRef](#)]
3. Price, R.E.; Savov, I.; Planer-Friedrich, B.; Buhring, S.I.; Amend, J.; Pichler, T. Processes influencing extreme As enrichment in shallow-sea hydrothermal fluids of Milos Island, Greece. *Chem. Geol.* **2013**, *348*, 15–26. [[CrossRef](#)]
4. Chen, X.G.; Lyu, S.S.; Garbe-Schonberg, D.; Lebrato, M.; Li, X.H.; Zhang, H.Y.; Zhang, P.P.; Chen, C.T.A.; Ye, Y. Heavy metals from Kueishantao shallow-sea hydrothermal vents, offshore northeast Taiwan. *J. Mar. Syst.* **2018**, *180*, 211–219. [[CrossRef](#)]
5. Hung, J.J.; Yeh, H.Y.; Peng, S.H.; Chen, C.T.A. Influence of submarine hydrothermalism on sulfur and metal accumulation in surface sediments in the Kueishantao venting field off northeastern Taiwan. *Mar. Chem.* **2018**, *198*, 88–96. [[CrossRef](#)]
6. Tang, K.; Zhang, Y.; Lin, D.; Han, Y.; Chen, C.T.A.; Wang, D.; Lin, Y.S.; Sun, J.; Zheng, Q.; Jiao, N.Z. Cultivation-Independent and Cultivation-Dependent Analysis of Microbes in the Shallow-Sea Hydrothermal System Off Kueishantao Island, Taiwan: Unmasking Heterotrophic Bacterial Diversity and Functional Capacity. *Front. Microbiol.* **2018**, *9*, 279. [[CrossRef](#)]
7. Kitadai, N.; Nakamura, R.; Yamamoto, M.; Takai, K.; Yoshida, N.; Oono, Y. Metals likely promoted protometabolism in early ocean alkaline hydrothermal systems. *Sci. Adv.* **2019**, *5*, eaav7848. [[CrossRef](#)]
8. Aquilina, A.; Connelly, D.P.; Copley, J.T.; Green, D.R.H.; Hawkes, J.A.; Hepburn, L.E.; Huvenne, V.A.I.; Marsh, L.; Mills, R.A.; Tyler, P.A. Geochemical and Visual Indicators of Hydrothermal Fluid Flow through a Sediment-Hosted Volcanic Ridge in the Central Bransfield Basin (Antarctica). *PLoS ONE* **2013**, *8*, e54686. [[CrossRef](#)]
9. Morowitz, H.J.; Srinivasan, V.; Smith, E. Ligand Field Theory and the Origin of Life as an Emergent Feature of the Periodic Table of Elements. *Biol. Bull.* **2010**, *219*, 1–6. [[CrossRef](#)]
10. He, D.T.; Liu, Y.S.; Moynier, F.; Foley, S.F.; Chen, C.F. Platinum group element mobilization in the mantle enhanced by recycled sedimentary carbonate. *Earth Planet Sci. Lett.* **2020**, *541*, 116262. [[CrossRef](#)]
11. Cai, R.H.; Liu, J.G.; Pearson, D.G.; Li, D.X.; Xu, Y.; Liu, S.A.; Chu, Z.Y.; Chen, L.H.; Li, S.G. Oxidation of the deep big mantle wedge by recycled carbonates: Constraints from highly siderophile elements and osmium isotopes. *Geochim. Cosmochim. Acta* **2021**, *295*, 207–223. [[CrossRef](#)]
12. Li, Y.F.; Tang, K.; Zhang, L.B.; Zhao, Z.H.; Xie, X.B.; Chen, C.T.A.; Wang, D.; Jiao, N.Z.; Zhang, Y. Coupled Carbon, Sulfur, and Nitrogen Cycles Mediated by Microorganisms in the Water Column of a Shallow-Water Hydrothermal Ecosystem. *Front. Microbiol.* **2018**, *9*, 2718. [[CrossRef](#)]
13. Lin, Y.S.; Lin, H.T.; Wang, B.S.; Huang, W.J.; Lin, L.H.; Tsai, A.Y. Intense but variable autotrophic activity in a rapidly flushed shallow-water hydrothermal plume (Kueishantao Islet, Taiwan). *Geobiology* **2021**, *19*, 87–101. [[CrossRef](#)] [[PubMed](#)]
14. Leal-Acosta, M.L.; Shumilin, E.; Mirlean, N.; Delgadillo-Hinojosa, F.; Sanchez-Rodriguez, I. The impact of marine shallow-water hydrothermal venting on arsenic and mercury accumulation by seaweed *Sargassum sinicola* in Concepcion Bay, Gulf of California. *Environ. Sci. Process. Impacts* **2013**, *15*, 470–477. [[CrossRef](#)]
15. Villanueva-Estrada, R.E.; Prol-Ledesma, R.M.; Rodriguez-Diaz, A.A.; Canet, C.; Armienta, M.A. Arsenic in hot springs of Bahia Concepcion, Baja California Peninsula, Mexico. *Chem. Geol.* **2013**, *348*, 27–36. [[CrossRef](#)]
16. Yu, M.Z.; Chen, X.G.; Garbe-Schonberg, D.; Ye, Y.; Chen, C.T.A. Volatile Chalcophile Elements in Native Sulfur from a Submarine Hydrothermal System at Kueishantao, Offshore NE Taiwan. *Minerals* **2019**, *9*, 245. [[CrossRef](#)]
17. Peng, S.H.; Hung, J.J.; Hwang, J.S. Bioaccumulation of trace metals in the submarine hydrothermal vent crab *Xenograpsus testudinatus* off Kueishan Island, Taiwan. *Mar. Pollut. Bull.* **2011**, *63*, 396–401. [[CrossRef](#)] [[PubMed](#)]
18. Zeng, Z.G.; Ma, Y.; Wang, X.Y.; Chen, C.T.A.; Yin, X.B.; Zhang, S.P.; Zhang, J.L.; Jiang, W. Elemental compositions of crab and snail shells from the Kueishantao hydrothermal field in the southwestern Okinawa Trough. *J. Mar. Syst.* **2018**, *180*, 90–101. [[CrossRef](#)]
19. Dahms, H.U.; Hwang, J.S. Mortality in the Ocean—With Lessons from Hydrothermal Vents Off Kueishan Tao, Ne-Taiwan. *J. Mar. Sci. Tech.* **2013**, *21*, 711–715.
20. Chan, B.K.K.; Wang, T.W.; Chen, P.C.; Lin, C.W.; Chan, T.Y.; Tsang, L.M. Community Structure of Macrobiota and Environmental Parameters in Shallow Water Hydrothermal Vents off Kueishan Island, Taiwan. *PLoS ONE* **2016**, *11*, e0148675. [[CrossRef](#)]
21. Mantha, G.; Awasthi, A.K.; Al-Aidaros, A.M.; Hwang, J.S. Diversity and abnormalities of cyclopoid copepods around hydrothermal vent fluids, Kueishantao Island, north-eastern Taiwan. *J. Nat. Hist.* **2013**, *47*, 685–697. [[CrossRef](#)]
22. Hsiao, S.H.; Fang, T.H. Hg bioaccumulation in marine copepods around hydrothermal vents and the adjacent marine environment in northeastern Taiwan. *Mar. Pollut. Bull.* **2013**, *74*, 175–182. [[CrossRef](#)]
23. Franco, P.; Dahms, H.U.; Hwang, J.S. Pelagic tunicates at shallow hydrothermal vents of Kueishantao. *PLoS ONE* **2019**, *14*, e0225387. [[CrossRef](#)]
24. Gartman, A.; Findlay, A.J. Impacts of hydrothermal plume processes on oceanic metal cycles and transport. *Nat. Geosci.* **2020**, *13*, 396–402. [[CrossRef](#)]
25. Chiu, C.L.; Song, S.R.; Hsieh, Y.C.; Chen, C.X. Volcanic Characteristics of Kueishantao in Northeast Taiwan and Their Implications. *Terr. Atmos. Ocean. Sci.* **2010**, *21*, 575–585. [[CrossRef](#)]
26. Chen, Y.G.; Wu, W.S.; Chen, C.H.; Liu, T.K. A date for volcanic eruption inferred from a siltstone xenolith. *Quat. Sci. Rev.* **2001**, *20*, 869–873. [[CrossRef](#)]

27. Zeng, Z.G.; Liu, C.H.; Chen, C.T.A.; Yin, X.B.; Chen, D.G.; Wang, X.Y.; Wang, X.M.; Zhang, G.L. Origin of a native sulfur chimney in the Kueishantao hydrothermal field, offshore northeast Taiwan. *Sci. China Ser. D* **2007**, *50*, 1746–1753. [[CrossRef](#)]
28. Wang, D.; Lin, W.F.; Yang, X.Q.; Zhai, W.D.; Dai, M.H.; Chen, C.T.A. Occurrences of dissolved trace metals (Cu, Cd, and Mn) in the Pearl River Estuary (China), a large river-groundwater-estuary system. *Cont. Shelf Res.* **2012**, *50–51*, 54–63. [[CrossRef](#)]
29. Pai, S.-C.; Whung, P.-Y.; Lai, R.-L. Pre-concentration efficiency of chelex-100 resin for heavy metals in seawater: Part 1. Effects of pH and Salts on the Distribution Ratios of Heavy Metals. *Anal. Chim. Acta* **1988**, *211*, 257–270. [[CrossRef](#)]
30. Lee, H.F.; Yang, T.F.; Lan, T.F.; Song, S.R.; Tsao, S. Fumarolic gas composition of the Tatun Volcano Group, northern Taiwan. *Terr. Atmos. Ocean Sci.* **2005**, *16*, 843–864. [[CrossRef](#)]
31. Parsons, T.R. Determination of chlorophylls and total carotenoids: Spectrophotometric method. In *A Manual of Chemical & Biological Methods for Seawater Analysis*; Pergamon Press: Oxford, UK, 1984; pp. 101–104.
32. Findlay, A.J.; Gartman, A.; Shaw, T.J.; Luther, G.W. Trace metal concentration and partitioning in the first 1.5 m of hydrothermal vent plumes along the Mid-Atlantic Ridge: TAG, Snakepit, and Rainbow. *Chem. Geol.* **2015**, *412*, 117–131. [[CrossRef](#)]
33. Mottl, M.J. Metabasalts, axial hot springs, and the structure of hydrothermal systems at mid-ocean ridges. *Geol. Soc. Am. Bull.* **1983**, *94*, 161–180. [[CrossRef](#)]
34. Rudnicki, M.D.; Elderfield, H. A Chemical-Model of the Buoyant and Neutrally Buoyant Plume above the Tag Vent Field, 26 Degrees-N, Mid-Atlantic Ridge. *Geochim. Cosmochim. Acta* **1993**, *57*, 2939–2957. [[CrossRef](#)]
35. Konstantinou, K.I.; Pan, C.Y.; Lin, C.H. Microearthquake activity around Kueishantao island, offshore northeastern Taiwan: Insights into the volcano-tectonic interactions at the tip of the southern Okinawa Trough. *Tectonophysics* **2013**, *593*, 20–32. [[CrossRef](#)]
36. Lin, Y.S.; Lee, J.; Lin, L.H.; Fu, K.H.; Chen, C.T.A.; Wang, Y.H.; Lee, I.H. Biogeochemistry and dynamics of particulate organic matter in a shallow-water hydrothermal field (Kueishantao Islet, NE Taiwan). *Mar. Geol.* **2020**, *422*, 106121. [[CrossRef](#)]